Journal of Alloys and Compounds 517 (2012) 45–53

Contents lists available at SciVerse ScienceDirect

Journal of Alloys and Compounds

journal homepage: www.elsevier.com/locate/jallcom

Evaluation of strengthening behavior of Al–AlN nanostructured composite by the use of modified Heckel model and response surface methodology

Hamidreza Farnoush[a,*], Davoud Haghshenas Fatmehsari[a], Jamshid Aghazadeh Mohandesi[a], Hamid Abdoli[b]

[a] Department of Mining and Metallurgical Engineering, Amirkabir University of Technology, P.O. Box 15875-4413, Tehran, Iran
[b] Department of Materials Science and Engineering, Tarbiat Modares University, P.O. Box 1411-5143, Tehran, Iran

ARTICLE INFO

Article history:
Received 11 July 2011
Received in revised form
25 November 2011
Accepted 28 November 2011
Available online 6 December 2011

Keywords:
Nanostructured materials
Aluminum matrix composites
Mechanical alloying
Compressibility
Response surface methodology
Yield strength

ABSTRACT

Al–AlN powder mixtures with 0, 5 and 10 wt.% of AlN were mechanically alloyed in a planetary ball mill under argon atmosphere up to 25 h. The compressibility behavior of the obtained samples was investigated in a wide range of compaction pressure from 62.5 up to 875 MPa. It was shown that presence of 10 wt.% of AlN leads to a reduction in the rate of hardening after 15 h milling. The morphological features of the samples showed that after 15 and 25 h milling, a relative steady-state equiaxed powder can be synthesized in the case of Al–10% AlN and Al–5% AlN, respectively. A combined modified Heckel model and response surface methodology (RSM) based on central composite design (CCD) was also employed to study the effect of three factors of AlN wt.%, milling time and compaction pressure on the densification and strengthening behavior of nanostructured Al–AlN composites. All the three factors had statistically significant effect on density (D) and yield strength (YS); while in the case of milling strengthening fraction (MSF) as the response, AlN was statistically insignificant. Second order polynomial models were successfully fitted to the responses in different ranges of low (125–375 MPa) and high (625–875 MPa) pressures. Furthermore, the statistically significant interactions between parameters were comprehensively discussed in each case.

1. Introduction

Aluminum nitride (AlN) nanoparticles, as the reinforcement, can effectively enhance the properties of aluminum matrix composites (AMCs) [1–3]. The advantages of AlN, over other reinforcements such as SiC [4–6], Al_2O_3 [7–12], TiC [13], TiB_2 [14], and B_4C [15], are not reacting with molten aluminum, excellent conductivity, low thermal expansion coefficient, high strength and, good oxidation resistance at elevated temperatures [2,16,3].

Mechanical alloying (MA) is one of the reasonable and effectual techniques for the fabrication of nanostructured Al–AlN composite with a homogenous distribution of the reinforcement particles at ambient temperature [17]. The formation of such homogenous composite powders is the result of repetitive welding–fracturing–welding occurred in a high-energy ball mill [8,18,19]. Hereafter, cold compaction followed by sintering can be practically applied for the production of full dense compacts [20–22].

It has been reported that a four-stage mechanism is responsible for particle compaction [23–25]; the volume decrease due to the slippage between particles/or rearrangement, the plastic flow of ductile particles, the fragmentation of work-hardened powders, and the elastic deformation of bulk composite. The influential factors on the compressibility behavior of materials have been extensively investigated including intrinsic characteristics of the material [26], deformability [27], morphology [11], inter-particle and particle/die wall friction [28], particle size and volume fraction of the reinforcements [11,29,30], and lubricating [31].

Abdoli et al. [17,32] have attempted to correlate the relative density of Al–AlN nanostructured composites with the applied pressure using different models. They showed that conventional models [33,34] cannot precisely reproduce the experimental data because of the different densification mechanisms at various range of compacting pressures. However, the modified Heckel equation [32,35] could result in more acceptable predictions due to considering the constraint caused by neighboring particles [36].

In Table 1, the mathematical equations of the models employed in our previous works [17,32], are listed; in these relations D, P, ν and K are the relative density, the applied pressure, Poisson's ratio and plastic deformation capacity of the material (varies with one-third of inverse the yield strength (σ_0)), respectively; and D_0 is the

* Corresponding author. Tel.: +98 21 64542949; fax: +98 21 64542941.
E-mail address: farnoush@aut.ac.ir (H. Farnoush).

0925-8388/$ – see front matter © 2011 Elsevier B.V. All rights reserved.
doi:10.1016/j.jallcom.2011.11.138

Table 1
Empirical compaction models used for Al–AlN nanostructured composites [17,32].

Model		
Heckel [33]	$\ln\left(\frac{1}{1-D}\right) = \ln\left(\frac{1}{1-D_0}\right) + KP, \quad K = \frac{1}{3\sigma_0}$	(1)
Panelli–Filho [34]	$\ln\left(\frac{1}{1-D}\right) = \ln\left(\frac{1}{1-D_0}\right) + KP^{1/2}$	(2)
Modified Heckel [35]	$\ln\left(\frac{1}{1-D}\right) = \ln\left(\frac{1}{1-D_0}\right) + \frac{1}{3k_1}\ln\left(1+\frac{k_1P}{\sigma_0}\right), \quad k_1 = \frac{2\nu^2}{1-2\nu}$	(3)

relative density at $P = 0$. The predictions resulted from Eqs. (1) and (2), are not in good agreement with those experimentally obtained because the effect of pressure on the yield strength is ignored. On the other hand, Denny [35] proposed a linear relationship between yield strength and applied pressure:

$$\sigma = \sigma_0 + k_1 P \tag{4}$$

where σ is the yield strength of consolidated materials. It was found that the initial strength of powder induced by mechanical alloying has a great impact on the final strength of powder compacts [37]. The effects of milling and compaction on the strengthening are described by Eq. (4); the effect of milling is reflected in σ_0 while the pressure dependency term, k_1P, describes the effect of compaction.

It is worthy of note that the correct identification of the effective factors in such systems can be achieved by an appropriate design of experiment. However, the optimum levels of milling parameters were not fully explained in previous works and, furthermore, the optimum level of these parameters might also be influenced by the level of the other important factors in the process. In statistical parlance, there might be an interaction between effective parameters in such a process. A survey of previous literature on ball milling systems provides no clues as to whether such interaction between the important process parameters exists or not. This is because in previous studies one-factor-at-a-time methodology has been used to optimize the above mentioned parameters [32,37]. This methodology is very inefficient and furthermore gives absolutely no information about interactions between parameters in a process. The only methodology capable of providing an answer to this question is factorial design of experiments (DOEs), which – through the use of techniques such as response surface methodology (RSM) – is able to simultaneously consider several factors at different levels, and give a suitable model for the relationship between the various factors and the response [38]. However, RSM has been applied in only one case to a ball milling system [39].

There are full as well as fractional factorial DOEs; the former gives the most complete information regarding interaction between parameters but the number of experiments becomes excessive when the number of factors or their levels becomes relatively large. Additionally, higher order interactions are usually statistically insignificant and, consequently, information about them is not very useful [38]. Fractional factorial designs (FFD) – such as central composite design (CCD) – can give information regarding parameter interactions with the use of less experimentation; however, reliable information about first order interactions can only be obtained from the results of DOEs which are not highly fractionated [38].

The aim of current work was to evaluate the effects of high-energy mechanical alloying and cold compaction on strengthening of nanostructured Al–AlN composites. A combination of modified Heckel model and a very common RSM, for first time, was used to predict strengthening of compacts. A half fractional factorial CCD was chosen as the design matrix since it allows reliable identification of first order interaction between factors and provides a second order polynomial model which can be used to predict optimum level of these parameters.

2. Experimental details

Al (100 μm, Merck Co., Whitehouse Station, NJ, USA) mixed with 0, 5 and 10 wt.% AlN (10 μm, Sigma–Aldrich Co., St Louis, MO, USA) powders were subjected to high-energy milling in a planetary ball-mill with 270 rpm rotational speed. The milling operation was carried out under argon atmosphere in 100 mm diameter hardened steel vials include 20 mm diameter chromium steel balls with 20:1 ball-to-powder ratio (BPR) and 1.5 wt.% stearic acid as a process control agent (PCA). Experimental details for characterization procedure of materials have been described elsewhere [17,32]. The 5, 10, 15, and 25 h milled powder mixtures were then compacted at 62.5, 125, 250, 375, 500, 625, 750, and 875 MPa pressures in a 10 mm diameter cylindrical die. Die wall lubrication should be afforded intermittently with using zinc stearate spray. The density of the green compacts was measured by Archimedes' technique to establish subsequent compressibility curves. Morphological features of the samples were followed by Philips XL30 scanning electron microscope (SEM).

Response surface methodology (RSM) was employed to investigate the effect of AlN wt.% (AlN), milling time (time) and compaction pressure (P) parameters on the density (D), yield strength (YS) and milling strengthening fraction (MSF). A central composite design (CCD) was adopted in this work to study three factors at three levels. Seventeen experimental runs consisting of 6 star points (star distance is 0) and 3 center points were generated with 3 factors and 3 levels by the principle of RSM using MINITAB Release 15. The CCD matrix employed for two pressure ranges (high and low ranges), which includes the levels employed for the different factors, is presented in Tables 2 and 3. The quadratic polynomial regression model, as follows, was chosen for predicting the response variable in terms of the four independent variables chosen for study [38]:

$$Y = b_0 + \sum_{i=1}^{4} b_i X_i + \sum_{i=1}^{4} b_{ii} X_i^2 + \sum_{i=1}^{3}\sum_{j=i+1}^{4} b_{ij} X_i X_j \tag{5}$$

In this equation Y is the response variable b_0, b_i, b_{ii}, and b_{ij} are constant coefficients of intercept, linear, quadratic and interaction terms, respectively, and X_i and X_j represent the four independent variables (P, time, AlN). The experiments were carried with two replicates and conducted in a randomized order to avoid systematic bias.

The statistical significance of the full quadratic models predicted was evaluated by the analysis of variance (ANOVA). The significance and the magnitude of the effects estimates of each variable and all their possible linear and quadratic

Table 2
Central composite design arrangement and responses (high pressure range).

Experiment number	Factors			Responses		
	AlN (wt.%)	Time (s)	P (MPa)	D	YS (MPa)	MSF
1	0	5	625	0.969	151.19	0.344
2	10	5	625	0.880	300.69	0.339
3	0	25	625	0.890	249.37	0.613
4	10	25	625	0.824	373.44	0.573
5	0	5	875	0.978	190.86	0.272
6	10	5	875	0.909	380.16	0.268
7	0	25	875	0.920	287.92	0.531
8	10	25	875	0.858	437.21	0.489
9	0	15	750	0.937	227.17	0.502
10	10	15	750	0.853	390.40	0.509
11	5	5	750	0.915	319.10	0.241
12	5	25	750	0.862	364.40	0.565
13	5	15	625	0.871	304.50	0.414
14	5	15	875	0.892	375.90	0.335
15	5	15	750	0.890	336.00	0.332
16	5	15	750	0.887	338.40	0.386
17	5	15	750	0.880	345.60	0.392

Table 3
Central composite design arrangement and responses (low pressure range).

Experiment number	Factors			Responses		
	AlN (wt.%)	Time (s)	P (MPa)	D	YS (MPa)	MSF
1	0	5	125	0.858	71.84	0.724
2	10	5	125	0.742	141.74	0.720
3	0	25	125	0.751	172.27	0.888
4	10	25	125	0.699	245.89	0.870
5	0	5	375	0.937	111.51	0.466
6	10	5	375	0.837	221.21	0.461
7	0	25	375	0.842	210.82	0.726
8	10	25	375	0.778	309.66	0.691
9	0	15	250	0.835	151.72	0.751
10	10	15	250	0.752	262.80	0.757
11	5	5	250	0.815	157.70	0.488
12	5	25	250	0.764	258.80	0.796
13	5	15	125	0.722	161.70	0.779
14	5	15	375	0.817	233.10	0.540
15	5	15	250	0.756	199.60	0.665
16	5	15	250	0.777	197.40	0.652
17	5	15	250	0.790	195.20	0.5972

interactions on the response variables were also determined. Finally, the model was used to predict the optimum value and to compare with the semi-empirical developed models.

3. Results and discussion

3.1. Development of the modified Heckel equation

Identification of the compressibility characteristics of milled powder mixtures in strengthening behavior of Al–AlN nanostructured composite is a prerequisite for a comprehensive investigation of the process. This is especially true when this evaluation has to compare with statistically based models. Regarding this issue, the results obtained by employing Heckel (Eq. (1)), Panelli–Filho (Eq. (2)), and modified Heckel (Eq. (3)) models are given in Table 4 which are a collection of previously reported data [17,32,37] and recently obtained data in the present work. Based on the values of correlation coefficients (R^2), the modified Heckel model conforms well to the experimental data compared to other models which can be attributed to the fact that this model considers the constraining effect of neighboring particles during compaction and its consequence of yield strength [36]. However, Fogagnolo et al. [40] used Panelli–Filho equation to estimate the plastic deformation capacity of Al6061–AlN powders during the compacting. As a matter of knowledge, there are two mechanisms involved in densification of metal powders: particle rearrangement (at low pressures) and plastic deformation (at high pressures) [24,25]; thus, the conventional Heckel model results in imprecise predictions at a wide range of pressure. Fig. 1 shows compressibility curves of milled powders fitted by modified Heckel model. As can be seen, the green density of compacts decreases by an increase in both AlN content and milling time which is due to the hardening effect of the mechanical milling [17,32]. It is also found that the final strength of powder compacts significantly depends on the initial strength of powder induced by mechanical alloying [37]. In fact, during compaction of strengthened powders it is difficult for soft particles to cover and fill the free spaces between hard particles [41,42]. Fig. 2 shows the variations of yield strength of Al, Al–5 wt.% AlN (Al5AlN) and Al–10 wt.% AlN (Al10AlN) compacts versus milling time in different ranges of pressure. As can be observed, the strengths of both Al and Al5AlN increase almost linearly with milling time, while that of Al10AlN has a parabolic form at all pressures.

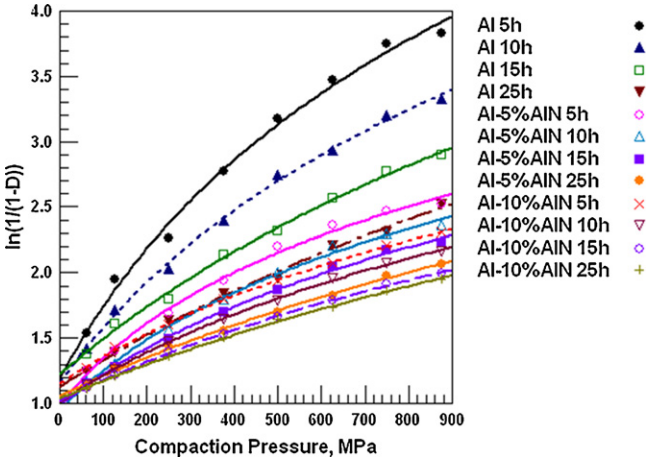

Fig. 1. Compressibility curves of Al and Al–AlN composite powders, showing the effects of reinforcement weight percent and milling time on densification.

The presence of a plateau region at high pressures (~875 MPa) shows a drastic reduction of strengthening rate in composite compacts. However, same behavior is expected for Al compacts at higher pressures (>875 MPa). According to Eq. (3), in strengthening process σ_0 and k_1P terms are the representatives of milling and compaction stages, respectively. Fig. 3 depicts the variation of milling strengthening fraction (σ_0/σ) versus milling time; the contribution of compaction stage in strengthening is much significant at both initial stages of milling and high pressures. In contrast, MSF rises sharply with milling time at lower compaction pressures. Furthermore, the strengthening arising from MA may be delayed in the absence of reinforcements. However, according to Fig. 3c, it seems that MA process have no effect on the strengthening of Al10AlN

Table 4
Comparison of compaction equations of nanostructured-Al–AlN composites.

% AlN	Milling time (h)	Modified Heckel					Panelli–Filho				Heckel			
		D_0	σ_0	K_1	R^2	Reference	D_0	$K\times10^{-2}$	R^2	Reference	D_0	$K\times10^{-3}$ (σ_0)	R^2	Reference
0	5	0.6952	52	0.1587	0.9928	[37]	0.4788	11.05	0.9901		0.7907	2.87 (116)	0.9619	
	10	0.6861	70	0.1762	0.9971	[37]	0.4957	9.02	0.9953		0.7597	2.35 (142)	0.9733	
	15	0.7053	114	0.1509	0.9961	[37]	0.5374	7.14	0.9901		0.7412	1.87 (178)	0.9847	
	25	0.6762	153	0.1542	0.9954	[17]	0.5239	5.79	0.99	[32]	0.7023	1.52 (219)	0.9898	[17]
5	5	0.6267	77	0.3228	0.9937	[37]	0.5176	6.3	0.9893		0.7143	1.63 (204)	0.9504	
	10	0.6138	96	0.3015	0.9945	[37]	0.488	5.89	0.9908		0.6853	1.53 (218)	0.9616	
	15	0.6274	126	0.2856	0.9972	[37]	0.5039	5.25	0.9939		0.6776	1.37 (243)	0.9747	
	25	0.6523	206	0.2112	0.9963	[32]	0.538	4.28	0.9919	[32]	0.6736	1.13 (296)	0.9905	[32]
10	5	0.6337	102	0.3179	0.9958		0.5211	5.58	0.9942		0.6978	1.45 (230)	0.9668	
	10	0.6347	146	0.28	0.999		0.517	4.85	0.9959		0.6751	1.27 (263)	0.982	
	15	0.6401	199	0.2552	0.9994		0.532	4.13	0.9939		0.6654	1.08 (308)	0.9894	
	25	0.6391	214	0.2551	0.9997	[17]	0.5349	3.93	0.9945	[32]	0.662	1.03 (323)	0.9921	[17]

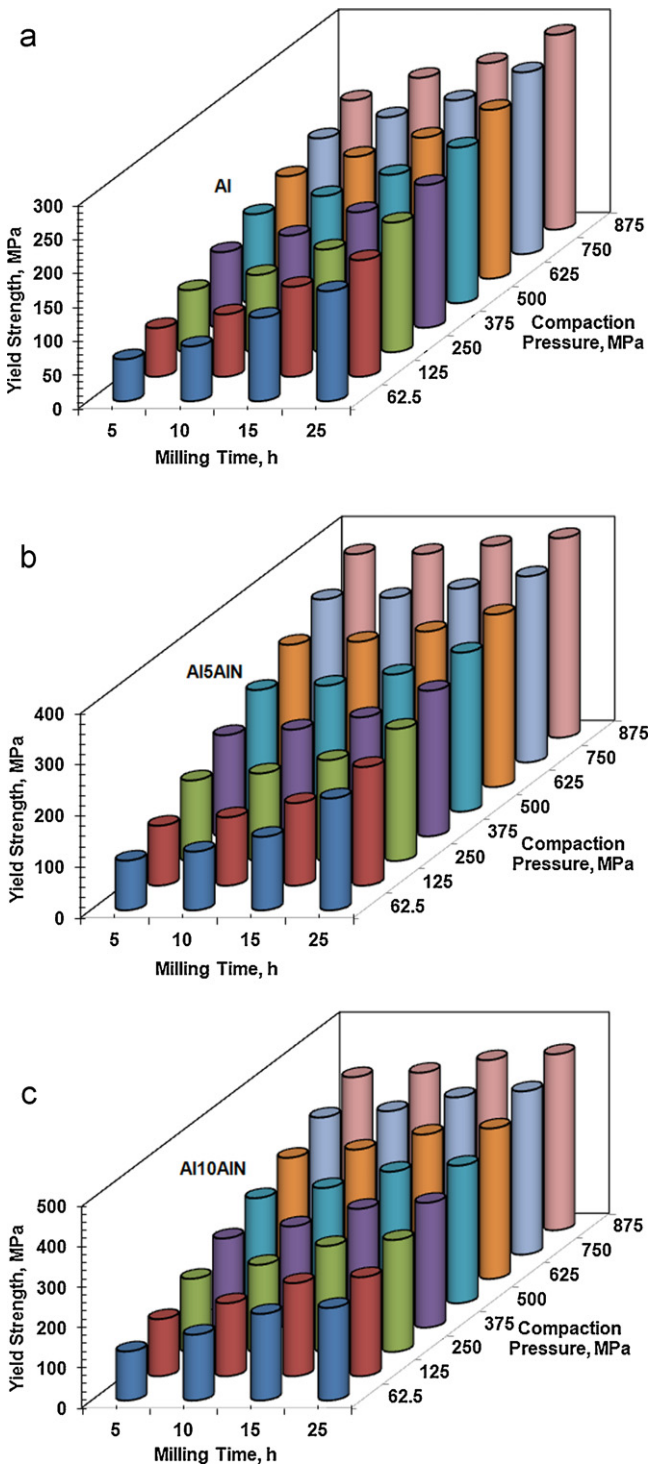

Fig. 2. Effect of milling time and compaction pressure on the yield strength of (a) Al, (b) Al5AlN, and (c) Al10AlN compacts.

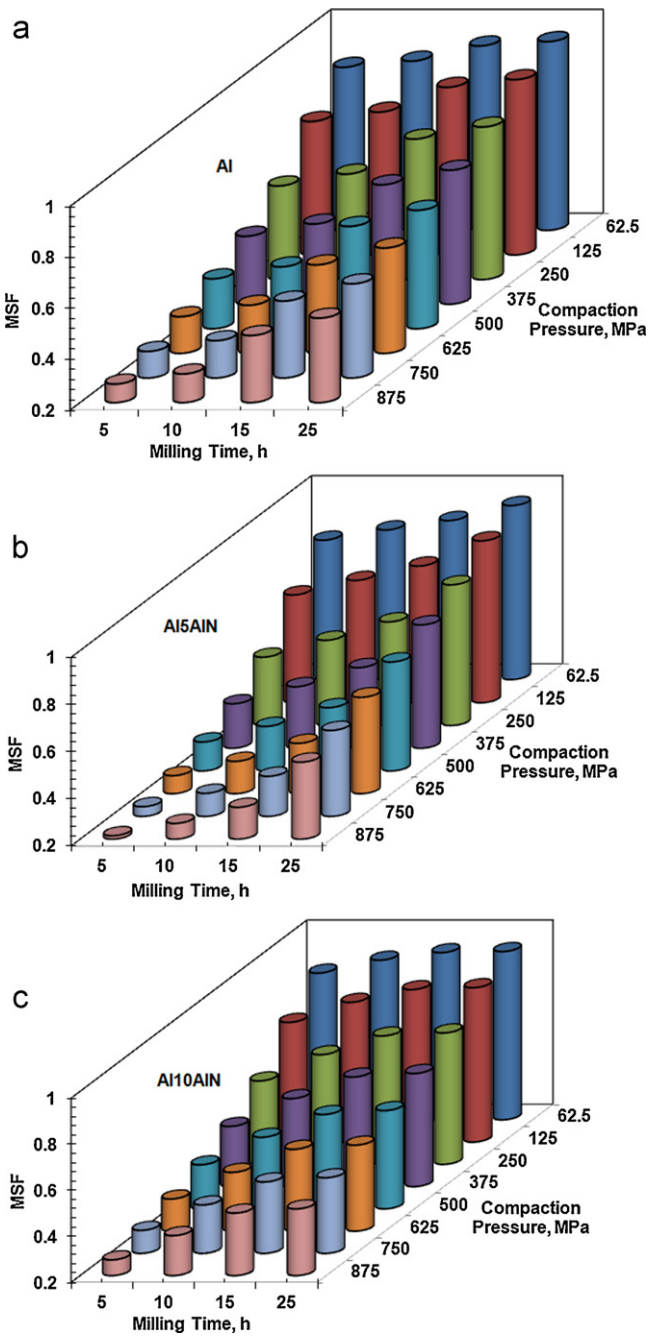

Fig. 3. Effect of milling time and compaction pressure on the milling strengthening fraction of (a) Al, (b) Al5AlN, and (c) Al10AlN compacts.

after 15 h milling. This is worthy of note that the lower densification rate of composite green compacts leads to insufficient density and sinterability after the consolidation process [22].

According to SEM images presented in Fig. 4 together with the detailed explanation of morphological evolution of the both milled monolithic powders (Al) and composite powders (Al–10 wt.% AlN) reported in Ref. [17], it can be deduced that only in the case of Al10AlN sample the steady-state morphology is attainable after 25 h milling. This result is further confirmed by the results presented in Fig. 3c, where the presence of 10 wt.% AlN particles leads to higher MSF at earlier times which is followed by a smooth rate after 15 h of milling. In contrast, as shown in Fig. 4b and c, incorporation of 5 wt.% AlN may prolong the time of steady-state condition; this result conforms to the linear variation of MSF within 10–25 h of milling (Fig. 3b).

3.2. Development of RSM-based polynomial quadratic models

Tables 2 and 3 list the values of responses at each of the 17 combination of factor levels generated by the principles of RSM. The results of the ANOVA are presented in Tables 5 and 6; the low p values for the regression ($p < 0.001$) and the fact that the lack of fit of the model was not significant ($p > 0.05$) indicates the suitability of the model.

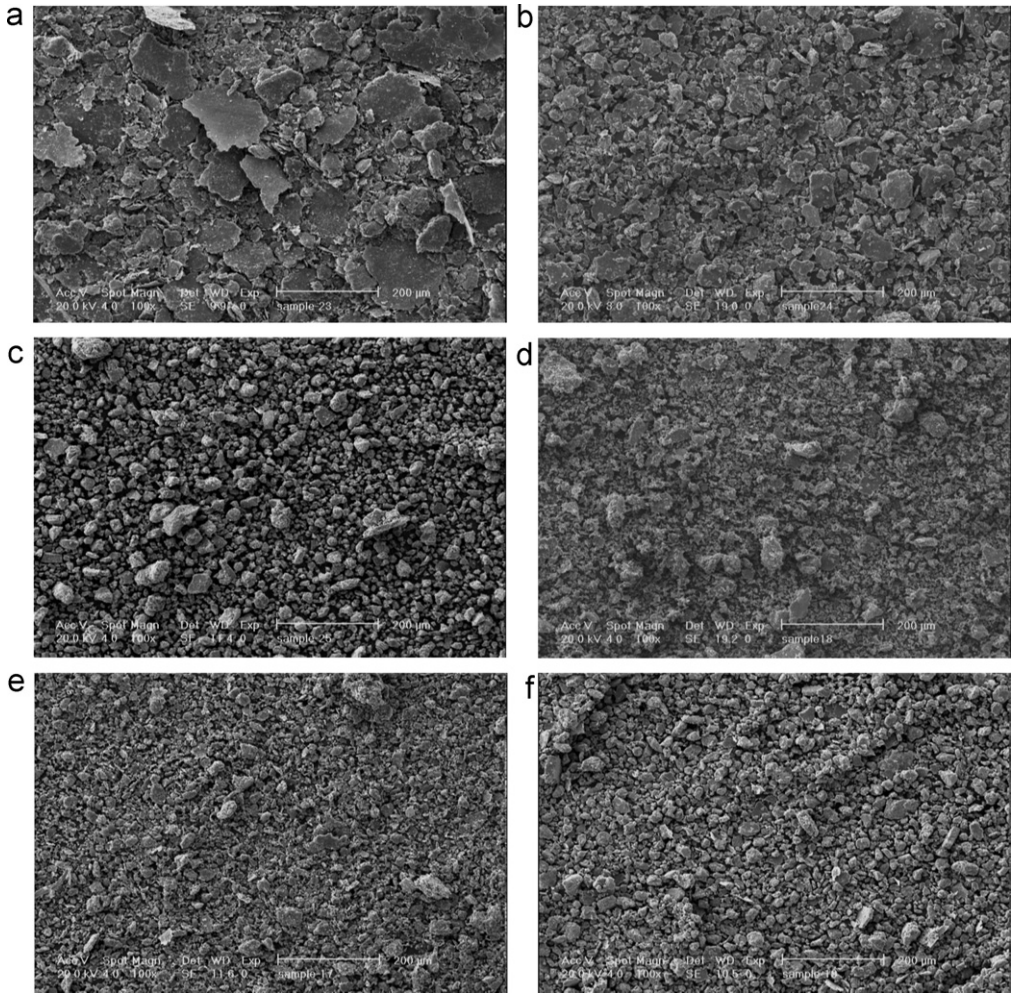

Fig. 4. Morphologies of Al5AlN (a–c) and Al10AlN (d–f) powder particles after (a and d) 10 h, (b and e) 15 h and (c and f) 25 h milling.

Table 5a
ANOVA table for *D* as the response (low pressure range).

	df	SS	MS	f-Values	*p*-Values
Total	16				
Regression	9	0.053749	0.005972	43.60	0.000
Residual error	7	0.000959	0.000137		
Lack of fit (model error)	5	0.000370	0.000074	0.25	0.908
Pure error (replicate error)	2	0.000589	0.000294		
R^2	95.99				

Abbreviations: df, degrees of freedom; SS, sum of squares; MS, mean square.

Table 5b
ANOVA table for YS as the response (low pressure range).

	df	SS	MS	f-Values	*p*-Values
Total	16				
Regression	9	55965.0	6218.3	178.12	0.000
Residual error	7	712.3	101.8		
Lack of fit (model error)	5	702.6	140.5	29.03	0.36
Pure error (replicate error)	2	9.7	4.8		
R^2	97.13				

Table 5c
ANOVA table for MSF as the response (low pressure range).

	df	SS	MS	f-Values	*p*-Values
Total	16				
Regression	9	0.267067	0.02967	20.56	0.000
Residual error	7	0.0101	0.00144		
Lack of fit (model error)	5	0.0075	0.00150	1.17	1.17
Pure error (replicate error)	2	0.0026	0.00129		
R^2	91.67				

Table 6a
ANOVA table for *D* as the response (high pressure range).

	df	SS	MS	f-Values	*p*-Values
Total	16				
Regression	9	0.02567	0.00285	96.15	0.000
Residual error	7	0.0002	0.00003		
Lack of fit (model error)	5	0.0001	0.00003	1.09	0.541
Pure error (replicate error)	2	0.00006	0.000028		
R^2	98.17				

Abbreviations: df, degrees of freedom; SS, sum of squares; MS, mean square.

Table 6b
ANOVA table for YS as the response (high pressure range).

	df	SS	MS	f-Values	*p*-Values
Total	16				
Regression	9	90860.1	10095.6	87.46	0.000
Residual error	7	808.0	115.4		
Lack of fit (model error)	5	758.1	151.6	6.07	0.147
Pure error (replicate error)	2	49.9	25.0		
R^2	97.99				

Table 6c
ANOVA table for MSF as the response (high pressure range).

	df	SS	MS	f-Values	*p*-Values
Total	16				
Regression	9	0.2103	0.0234	17.44	0.001
Residual error	7	0.0094	0.0013		
Lack of fit (model error)	5	0.0072	0.0014	1.33	0.483
Pure error (replicate error)	2	0.00212	0.0011		
R^2	90.24				

The value of the regression coefficients is presented in Tables 7 and 8. In the case of D and YS (as the responses), all the linear terms are significant, while AlN is insignificant for MSF (as the third response). The quadratic terms of AlN and time as well as the interactive terms of AlN and time shows significant statistical effect on D. The same statistical criterion ($p > 0.05$) can be applied for determination of effective linear and quadratic terms as well as their interactive terms.

Based on the regression coefficients calculated for the response (Tables 7 and 8) polynomial regression model equations were proposed as follows for high and low pressure ranges:

Low P range (125–375 MPa):

$$D = 0.850 - 0.019\ \ \mathrm{AlN} - 0.009\ \ \mathrm{time} + 3.5 \times 10^{-4}\ \ P + 7.3 \times 10^{-4}\ \ \mathrm{AlN}^2 + 1.5 \times 10^{-4}\ \ \mathrm{time}^2 + 2.5 \times 10^{-4}\ \ \mathrm{AlN} \times \mathrm{time} \quad (6)$$

$$\mathrm{YS} = -20.702 + 6.011\ \ \mathrm{AlN} + 4.934\ \ \mathrm{time} + 0.66\ \ P - 9.8 \times 10^{-4}\ \ P^2 + 0.013\ \ \mathrm{AlN} \times P \quad (7)$$

$$\mathrm{MSF} = 0.733 + 0.011\ \ \mathrm{time} - 8.77 \times 10^{-4}\ \ P \quad (8)$$

High P range (625–875 MPa):

$$D = 0.925 - 0.014\ \ \mathrm{AlN} - 0.005\ \ \mathrm{time} + 9.85 \times 10^{-5}\ \ P + 5 \times 10^{-4}\ \ \mathrm{AlN}^2 + 6.51 \times 10^{-5}\ \ \mathrm{time}^2 + 7.5 \times 10^{-5}\ \ \mathrm{AlN} \times \mathrm{time} \quad (9)$$

$$\mathrm{YS} = 26.52 + 24.89\ \ \mathrm{AlN} + 4.521\ \ \mathrm{time} + 0.169\ \ P - 1.67\ \ \mathrm{AlN}^2 - 0.164\ \ \mathrm{AlN} \times \mathrm{time} + 0.013\ \ \mathrm{AlN} \times P \quad (10)$$

$$\mathrm{MSF} = 0.454 + 0.013\ \ \mathrm{time} - 3.1 \times 10^{-4}\ \ P \quad (11)$$

3.3. Effects of parameters

In the cases where interaction between factors is statistically significant, contour plots give more complete information regarding the effect of a factor on the response. The simultaneous influences of reinforcement weight percent (AlN), milling duration (time) and compaction pressure (P) on green density (D), yield strength (YS) and milling strengthening fraction (MSF) can be identified using above developed models (RSM). As mentioned before, two different pressure ranges (i.e. 125–375 MPa and 625–875 MPa) were used to compare the role of each parameter during compaction. The general form of the above developed models can be re-written as:

$$D = A_0 + A_1\mathrm{AlN} + A_2\mathrm{time} + A_3P + A_{11}\mathrm{AlN}^2 + A_{22}\mathrm{time}^2 + A_{12}\mathrm{AlN} \times \mathrm{time} \quad (12)$$

$$\mathrm{YS} = B_0 + B_1\mathrm{AlN} + B_2\mathrm{time} + B_3P + B_{11}\mathrm{AlN}^2 + B_{33}P^2 + B_{12}\mathrm{AlN} \times \mathrm{time} + B_{13}\mathrm{AlN} \times P \quad (13)$$

$$\mathrm{MSF} = C_0 + C_2\mathrm{time} + C_3P \quad (14)$$

In Fig. 5, the values of regression coefficients calculated for responses are plotted which represents the significance of each term in both low and high compaction pressure ranges. As is known, during first stage of the consolidation process particle rearrangement (PR) mechanism prevails at low pressures, although plastic deformation (PD) gradually turns up after a critical stress [43].

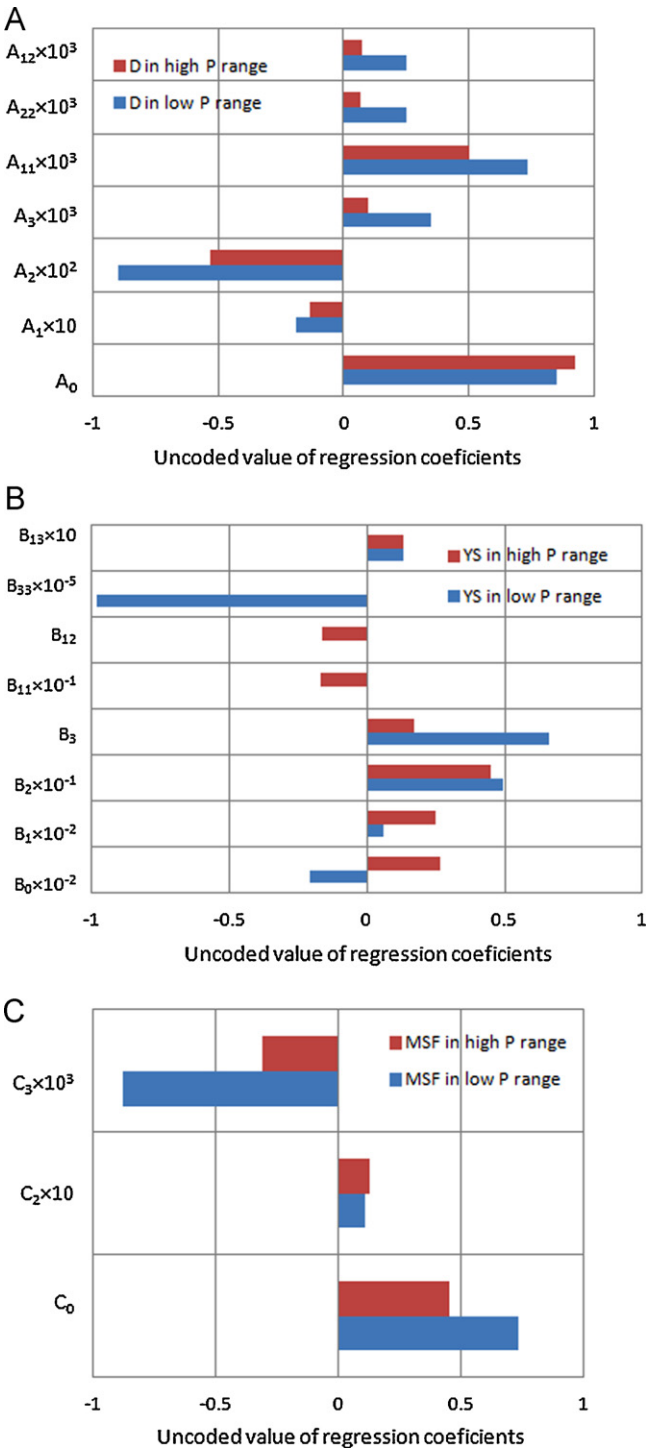

Fig. 5. Analysis of coefficients of (a) D, (b) YS, and (c) MSF in low and high pressure regions.

Reduction of density with AlN and time unlike incremental effect of pressure are summarized in A_1, A_2, and A_3, respectively (Eq. (12)). The quadratic term coefficients (A_{11}, A_{12}, and A_{22}) which lead to higher densities reveal the contribution of fine milled AlN particles in PR mechanism. According to Fig. 5a, in contrary to low pressure region, a higher densification (A_0) initially appears at the high pressure region, however, it drops to lower rates ($A_1, A_2, A_3, A_{11}, A_{12}$, and A_{22}). The effects of AlN, time, and P in Eq. (12), afford strengthened green compacts. The negative values of B_0, B_{33} together with the low value of B_1 in the low pressure region implies on the reverse

Table 7
Values of regression coefficients calculated for responses (low pressure range).

Independent factor	*D*			YS (MPa)			MSF		
	Regression coefficient	t-Value	*p*-Value	Regression coefficient	t-Value	*p*-Value	Regression coefficient	t-Value	*p*-Value
Constant	0.7738	154.525	0.000	204.723	47.428	0.000	0.6578	40.465	0.000
Linear									
AlN	−0.0414	−11.197	0.000	46.313	14.518	0.000	−0.0056	−0.466	0.655
time	−0.0356	−9.612	0.000	49.345	15.469	0.000	0.1112	9.257	0.000
P	0.04385	11.848	0.000	29.288	9.181	0.000	−0.110	−9.127	0.000
Quadratic									
AlN·AlN	0.0197	2.750	0.028	−2.952	−0.479	0.647	0.0819	3.529	0.010
time·time	0.0161	2.249	0.059	−1.964	−0.319	0.759	−0.0303	−1.304	0.234
P·*P*	−0.0038	−0.543	0.604	−12.814	−2.079	0.076	−0.0125	−0.539	0.607
Interactive									
AlN·time	0.01237	2.991	0.020	−0.894	−0.251	0.809	−0.0054	−0.400	0.701
AlN·*P*	0.0003	0.073	0.944	8.128	2.279	0.057	−0.0022	−0.166	0.873
time·*P*	−0.0007	−0.170	0.870	−2.103	−0.590	0.574	0.0218	1.624	0.149

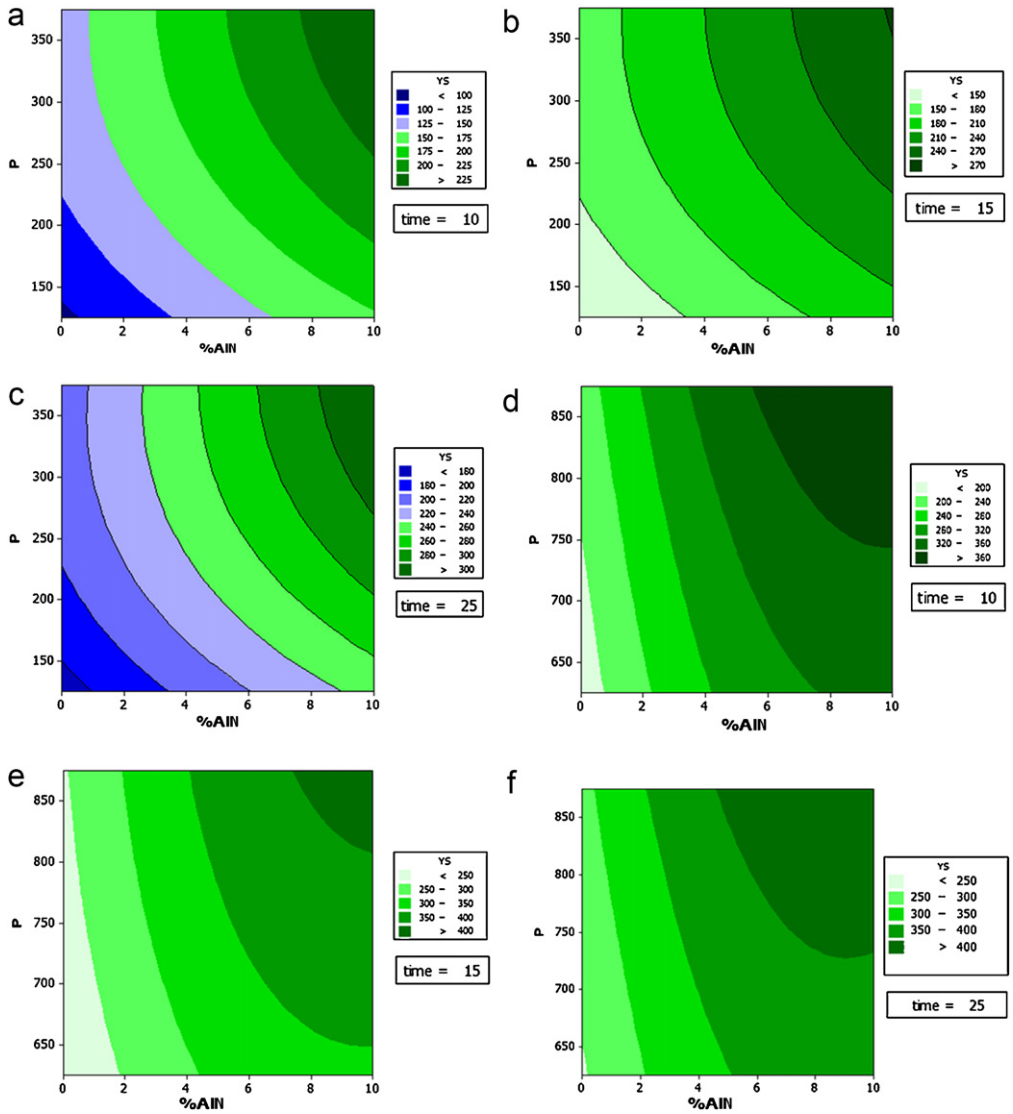

Fig. 6. Development of strengthening map by combined modified Heckel model and RSM corresponding to Al–AlN composites compacted in low (a–c) and high (d–f) pressure regions after (a and d) 10 h, (b and e) 15 h and (c and f) 25 h milling.

Table 8
Values of regression coefficients calculated for responses (high pressure range).

Independent factor	*D*			YS (MPa)			MSF		
	Regression coefficient	t-Value	*p*-Value	Regression coefficient	t-Value	*p*-Value	Regression coefficient	t-Value	*p*-Value
Constant	0.8836	379.163	0.000	343.241	74.661	0.000	0.3960	25.281	0.000
Linear									
AlN	−0.0372	−21.577	0.000	77.538	22.822	0.000	−0.0083	−0.720	0.495
time	−0.0297	−17.269	0.000	37.035	10.901	0.000	0.130753	11.294	0.000
P	0.0123	7.155	0.000	29.288	8.620	0.000	−0.0387	−3.341	0.012
Quadratic									
AlN·AlN	0.0130	3.923	0.006	−36.884	−5.619	0.001	0.0905	4.045	0.005
time·time	0.0066	1.973	0.089	−3.921	−0.597	0.569	−0.012	−0.536	0.609
P·P	−0.0002	−0.045	0.965	−5.471	−0.834	0.432	−0.041	−1.824	0.111
Interactive									
AlN·time	0.0038	1.950	0.092	−8.181	−2.154	0.068	−0.009	−0.710	0.501
AlN·*P*	0.0031	1.621	0.149	8.128	2.140	0.070	−0.00011	−0.008	0.994
time·*P*	0.0030	1.584	0.157	−2.103	−0.554	0.597	−0.0029	−0.225	0.828

effect of PR on yield strength (YS) of compacts (Fig. 5b). As a matter of knowledge, it is very likely that strengthening delays as the particles are more or less in a fixed arrangement. Although lower values of B_2 and B_3 in high pressure range explains the reduced hardening rate in compaction stage, the negative sign of both AlN × time and AlN × AlN in Eq. (13) indicates lower strengthening capacity after milling stage and filling effects of fine particles. The equation corresponded to MSF (Eq. (14)) shows that strengthening fraction of milling depends on both time and *P*. The statistical insignificancy of AlN observed in Eq. (14) can be potentially ascribed to the issue that the hardening effect of AlN reinforcement would rather be an equal fraction of strengthening in both milling and compaction stages. Due to reduced rate of hardening at higher pressures together with the prior-milling interference in strengthening capacity, higher values of C_0 and C_3 and lower value of C_2 are estimated (Fig. 5c).

Fig. 6 illustrates the bilateral effect of *P* and AlN on iso-yield strength curves evaluated by combining RSM and modified Heckel model after 10, 15, and 25 h milling. To verify the strengthening behavior of different compacts, the plots are established for two levels of pressure (high and low ranges). In high pressure region (Fig. 6d–f), hardening effect due to compaction pressure is somewhat insignificant but is mostly AlN-dependent. At low pressure region, in contrary, the increase in strength of compacts is influenced by both *P* and AlN (Fig. 6a–c). In low pressure region (>300 MPa) after 25 h milling, strengthening depends merely on AlN (Fig. 6c). Consequently, higher compaction pressure and/or 25 h prior-milling lead to a reduced hardening rate which is AlN dependent.

4. Conclusions

Densification and strengthening of nanostructured Al–AlN composites was investigated using a modified Heckel equation based on a statistical strategy. The effects of AlN reinforcement, milling time, and compaction pressure on compressibility and yield strength of compacts were studied. It has been found that hardening rate of Al10AlN varies smoothly after 15 h milling which confirms the steady-state condition of morphological evolutions. The presence of 10 wt.% of AlN particles accelerates the fragmentation, thus, finer equiaxed particles were obtained after 15 h milling; however an increasing rate of strengthening was observed after 25 h milling of Al5AlN particles.

Regarding two possible active mechanisms during compaction at low and high pressure ranges, namely as particle rearrangement and plastic deformation, a CCD coupled with RSM was employed to study the interaction between above mentioned parameters with the following results:

- The quadratic term coefficients in *D* as the response, which results in higher densities, implies on the contribution of fine milled AlN particles in PR mechanism.
- The statistical analysis shows that despite an initial higher densification at the high pressure region, its rate of variation drops drastically with compaction pressure.
- Furthermore, in the low pressure region the initial negative value of YS as the response indicates the reverse effect of PR.
- The negative sign of both interactive coefficient between AlN and time, and quadratic coefficient of AlN shows the lower strengthening capacity after milling stage and filling effects of fine particles.
- Additionally, as hardening effect of AlN reinforcement would rather be an equal fraction of strengthening in both milling and compaction stages, AlN term was statistically insignificant in MSF response.

References

[1] S.S. Sreeja Kumari, U.T.S. Pillai, B.C. Pai, J. Alloys Compd. 509 (2011) 2503–2509.
[2] H. Abdoli, E. Saebnouri, S.K. Sadrnezhaad, M. Ghanbari, T. Shahrabi, J. Alloys Compd. 490 (2010) 624–630.
[3] Y.Q. Liu, H.T. Cong, W. Wang, C.H. Sun, H.M. Cheng, Mater. Sci. Eng. A 505 (2009) 151–156.
[4] L. Kollo, M. Leparoux, C.R. Bradbury, C. Jäggi, E. Carreño-Morelli, M. Rodríguez-Arbaizar, J. Alloys Compd. 489 (2010) 394–400.
[5] S.A. Khadem, S. Nategh, H. Yoozbashizadeh, J. Alloys Compd. 509 (2011) 2221–2226.
[6] Y. Saberi, S.M. Zebarjad, G.H. Akbari, J. Alloys Compd. 484 (2009) 637–640.
[7] M. Alizadeh, M.M. Aliabadi, J. Alloys Compd. 509 (2011) 4978–4986.
[8] C. Suryanarayana, J. Alloys Compd. 509S (2011) S229–S234.
[9] S.A. Sajjadi, M. Torabi Parizi, H.R. Ezatpoura, A. Sedghic, J. Alloys Compd. 511 (2012) 226–231.
[10] J. Safari, G.H. Akbari, A. Shahbazkhanc, M. Delshad Chermahinid, J. Alloys Compd. 509 (2011) 9419–9424.
[11] S.S. Razavi-Tousia, R. Yazdani-Rad, S.A. Manafia, J. Alloys Compd. 509 (2011) 6489–6496.
[12] H. Ahamed, V. Senthilkumar, J. Alloys Compd. 505 (2010) 772–782.
[13] N. Nemati, R. Khosroshahi, M. Emamy, A. Zolriasatein, Mater. Des. 32 (2011) 3718–3729.
[14] Z. Sadeghian, B. Lotfi, M.H. Enayati, P. Beiss, J. Alloys Compd. 509 (2011) 7758–7763.
[15] M. Khakbiz, F. Akhlaghi, J. Alloys Compd. 479 (2009) 334–341.
[16] K. Mizuuchi, K. Inoue, Y. Agari, T. Nagaoka, M. Sugioka, M. Tanaka, T. Takeuchi, J. Tani, M. Kawahara, Y. Makino, M. Ito, Compos. B: Eng. (2011), doi:10.1016/j.compositesb.2011.06.017.
[17] H. Abdoli, E. Salahi, H. Farnoush, K. Pourazrang, J. Alloys Compd. 461 (2008) 166–172.
[18] J.B. Fogagnolo, E.M. Ruiz-Navas, M.H. Robert, J.M. Torralba, Mater. Sci. Eng. A 342 (2003) 131–143.
[19] M. Kubota, J. Alloys Compd. 504S (2010) S319–S322.
[20] S. Sivasankaran, K. Sivaprasad, R. Narayanasamy, V.K. Iyer, J. Alloys Compd. 491 (2010) 712–721.
[21] A. Glage, R. Ceccato, I. Lonardelli, F. Girardi, F. Agresti, G. Principi, A. Molinari, S. Gialanella, J. Alloys Compd. 478 (2009) 273–280.
[22] H. Abdoli, H. Asgharzadeh, E. Salahi, J. Alloys Compd. 473 (2009) 116–122.
[23] T. Çomoglu, J. Fac. Pharm. 36 (2007) 123–133.

[24] H.R. Hafizpour, A. Simchi, S. Parvizi, Adv. Powder Technol. 21 (2010) 273–278.
[25] S. Sivasankaran, K. Sivaprasad, R. Narayanasamy, V.K. Iyer, Powder Technol. 209 (2011) 124–137.
[26] Y. Guo, C.-Y. Wu, C. Thornton, Chem. Eng. Sci. 66 (2011) 661–673.
[27] S. Sivasankaran, K. Sivaprasad, R. Narayanasamy, Mater. Sci. Eng. A 528 (2011) 6776–6787.
[28] M. Olsson, U. Bexell, Wear 271 (2011) 1903–1908.
[29] T.W. Kim, Mater. Sci. Eng. A 483/484 (2008) 648–651.
[30] C.A. Leon, G. Rodriguez-Ortiz, E.A. Aguilar-Reyes, Mater. Sci. Eng. A 526 (2009) 106–112.
[31] G. Léonard, N. Abatzoglou, Powder Technol. 208 (2011) 54–62.
[32] H. Abdoli, H. Farnoush, E. Salahi, K. Pourazrang, Mater. Sci. Eng. A 486 (2008) 580–584.
[33] R.W. Heckel, Trans. Metall. Soc. AIME 221 (1961) 671–675.
[34] R. Panelli, F.A. Filho, Powder Technol. 114 (2000) 255–261.
[35] P.J. Denny, Powder Technol. 127 (2002) 162–172.
[36] L. Peter Martin, A.M. Hodge, G.H. Campbell, Scripta Mater. 57 (2007) 229–232.
[37] H. Abdoli, H.R. Farnoush, H. Asgharzadeh, S.K. Sadrnezhaad, Powder Metall. 54 (2011) 24–29.
[38] D.C. Montgomery, Design and Analysis of Experiments, 6th ed., John Wiley & Sons, New York, 2006.
[39] M. Rezaee, S.M.M. Khoie, D. Haghshenas Fatmehsari, H.K. Liu, J. Alloys Compd. 509 (2011) 8912–8916.
[40] J.B. Fogagnolo, E.M. Ruiz-Navas, M.H. Roberta, J.M. Torralba, Mater. Sci. Eng. A (2003) 50–55.
[41] W. Wu, G. Jiang, R.H. Wagoner, G.S. Daehn, Acta Mater. 48 (2000) 4323–4330.
[42] G. Jiang, W. Wu, G.S. Daehn, R.H. Wagoner, Acta Mater. 48 (2000) 4331–4335.
[43] K. Kondoh, R. Watanabe, H. Hashimoto, Powder Metall. 43 (2000) 359–363.